Structural analysis of premolar roots in Middle Pleistocene hominins from China

Lei Pan, Jean Dumoncel, Arnaud Mazurier, Clément Zanolli

Structural analysis of premolar roots in Middle Pleistocene hominins from China

Abstract:

This study investigates permanent maxillary and mandibular premolar root structural organization in East Asian Middle Pleistocene hominins. In addition to analyzing the linear and volumetric properties of the roots, we used a landmark-free approach to both qualify and quantify in 3D premolar root shape variation of Middle Pleistocene hominins in East Asia. Moreover, we focus on some mid- to late East Asian Middle Pleistocene hominin specimens whose taxonomic attribution is unclear. We find considerable cementum in this sample of hominins, similar to other fossil groups, but clearly different from modern humans which have a very small amount of cementum. Additionally, a smaller root pulp cavity is found in later *Homo* (Neanderthals and modern humans). Our analyses on the crown-root surface area ratio show that East Asian Middle Pleistocene *H. erectus* as well as one late Middle Pleistocene *Homo* sp. specimen (PA 81 P_4 from Changyang site) are distinguished from other fossil and extant groups by relatively larger root surface, stout root branches and thick cementum deposits. This may represent a distinct East Asian *H. erectus* dental pattern. Geometric morphometric analyses on the external root surface reveal a general trend of shape simplification along the *Homo* lineage examined here, and distinguish Early Pleistocene *Homo*, Middle Pleistocene *H. erectus*, Neanderthals and modern human morphologies. The late Middle Pleistocene teeth from Changyang site (PA 76 P^3 and PA 81 P^4) areclose to East Asian *H. erectus* and Neanderthals, while the mid-Middle Pleistocene P_3 from Panxian Dadong falls within the modern human distribution. Combined with dental crown morphology and root number/form reported in previous studies, our results show that the external root shape canbe considered a taxonomically relevant indicator. In general, an evolutionary tendency towards modern

human morphology is observed in part of the East Asian Middle Pleistocene specimens, while a retention of primitive, *H. erectus*-like features is expressed in some late Middle Pleistocene specimens, supporting a multi-lineage and discontinuous scenario of human settlements in East Asia.

Key words: East Asian Middle Pleistocene *Homo*; permanent premolar; external root surface; crown-root tissue proportions

1. Introduction

Hominin postcanine tooth root and canal anatomy is highly variable (e.g., Sert and Bayirli, 2004; Prado-Simón et al., 2012a; Kupczik et al., 2019). Using direct observation of the external roots (Turner, 1981; Spencer, 2003; Moggi-Cecchi et al., 2010), 2D radiography (Sperber, 1974; Abbott, 1984; Wood et al., 1988; Wood and Engleman, 1988), and medical/micro-tomography (Kupczik et al., 2003, 2005; Kupczik and Dean, 2008; Moore et al., 2013, 2015, 2016), studies have demonstrated that tooth roots preserve information about dietary adaptation, taxonomy and phylogeny (Abbott, 1984; Wood et al., 1988; Wood and Engleman, 1988; White et al., 2000; Le Cabec et al., 2013; Moore et al., 2016). In *Australopithecus*, *Paranthropus* and early *Homo* the plesiomorphic great-ape pattern is expressed by (1) three-rooted maxillary premolars with three canals, being supported by one lingual and two buccal roots, and (2) double-rooted mandibular premolars with three (P_3) or four (P_4) canals (Abbott, 1984; Wood et al., 1988; Emonet, 2009; Moore et al., 2013, 2015, 2016; Emonet et al., 2014). The derived modern human pattern is a reduced premolar root number and simplified root form, predominately represented by single-rooted premolars, even if variants such as double-rooted maxillary premolars and Tomes'-rooted mandibular premolars (Tomes' root refers to some lower premolars being C-shaped in cross section, which resulted from the radicular or developmental grooves of different levels that are considered to be associated with the evolution from multiple roots to single root) also

exist in modern human populations (e.g., Tomes, 1923; Loh, 1998; Sert and Bayirli, 2004; Shields, 2005; Dou et al., 2017; Scott et al., 2018).

in addition to quantitative investigations involving standard metrics such as root length, root surface area, cervical area and root volume (Kupczik and Hublin, 2010; Le Cabec et al., 2012, 2013; Moore et al., 2013, 2015, 2016; Kupczik et al., 2019), advances in X-ray microtomographic (micro CT) techniques have helped to characterize premolar root phenotypes and reveal previously undocumented variation in fossil hominins (e.g., Prado-Simón et al., 2012b; Kaifu et al., 2015; Moore et al., 2016; Liu et al., 2017).. Studies on primate postcanine roots reveal that the proportion of crown and root surface areais a useful proxy for both functional and phylogenetic assessments. For example, among *Gorilla gorilla*, *Pan troglodytes* and *P. pygmaeus*, *G. gorilla* has the largest relative postcanine root surface area, resulting in a larger attachment area that provides a functional advantage as it consumes mechanically resistant foods, and closely related species have similar crown-root area proportions (Kupczik et al., 2005, 2009; Kupczik and Dean, 2008). In contrast, landmark-based, 3D geometric morphometric (GM) analyses of root and cervix shape (Emonet et al., 2012; Moore et al., 2013; Kupczik et al., 2018) support a strong association between hominin taxonomy, phylogeny and root morphology. In spite of the fact that GM can quantify the 3D shape of the root better than standard linear and angular metrics, premolar root number and shape is highly variable, with few homologous landmarks that can be confidently placed (Emonet et al., 2012). To overcome such obstacles and explore 3-D root morphology, the present study employs a recently developed landmark-free approach (Durrleman et al., 2012a; Dumoncel et al., 2014; Beaudet et al., 2016; Zanolli et al., 2018; Braga et al., 2019) to quantify the entire external shape of the root in fossil hominins.

A recent non-metric investigation (Pan and Zanolli, 2019) using 2D virtual sections showed that among

Chinese Middle Pleistocene human dental remains, the expression of root/canal form could be roughly aligned in a chronological sequence -- the earliest specimens show an archaic morphology shared with *H. erectus* in Asia while the mid- to late Middle Pleistocene (296–194 Ka BP) group assigned to "archaic *H. sapiens*" shows a modern-like morphology (premolars exhibit symmetrical occlusal contour, simplified occlusal conformations, lack of cingulum, and gracile roots), while some archaic features are only weakly expressed (Liu et al., 2013; Xing et al., 2019). East Asian mid-Middle Pleistocene *H. erectus* populations show closer affinity to other Early and Middle Pleistocene hominins in Eurasia than to East African early *Homo* (Pan and Zanolli, 2019). The results of this previous study supported the hypothesis that at least some of the Early Pleistocene hominin groups in Eurasia may have contributed to modern human populations (Kaifu et al., 2005; Martinón-Torres et al., 2007). However, despite the growing evidence from tooth structural organization—including aspects on the outer enamel surface (OES) and enamel dentine junction (EDJ) morphology (e.g., Xing et al., 2016, 2018; Liu et al., 2017; Martinón-Torres et al., 2018; Zanolli et al., 2018)—it is still difficult to satisfactorily link a number of late Middle Pleistocene dental specimens to known hominin lineages (Chia, 1957; Bailey and Liu, 2010; Liu et al., 2013). To resolve this problem, morphological variation and evolutionary trends in the Chinese Middle Pleistocene fossil record needs to be further assessed. By using micro-CT scanning and 3D image processing techniques, this study aims at (1) report premolar root metrics, quantify crown-root tissue proportions, and investigate root geometric morphometrics of Middle Pleistocene hominins in East Asia; (2) evaluate the taxonomic and phylogenetic utility of external root shape in hominins, and assess evolutionary trends of premolar root morphology; and (3) , compare the few specimens with no clear taxonomic attribution (previously categorized as "archaic *H. sapiens*") to early to mid-Middle Pleistocene East Asian *H. erectus* premolars, as well as with those of other Pleistocene and recent

human groups from Africa and Eurasia, in order to shed light on their taxonomic status and eventually assess if multiple human lineages may have been living in East Asia during the Middle Pleistocene. Finally, this study will contribute to the discussion of the spatio-temporal distribution of the East Asian hominins.

2. Materials and Methods

2.1 Study sample

The Chinese Middle Pleistocene hominins consist of 11 premolars coming from six different localities and spanning the Middle Pleistocene (Table 1). This group is comprised of two samples. The first is Middle Pleistocene *H. erectus* (HEC, N=8) derived from Zhoukoudian and Chenjiawo sites and Xichuan county, with a chronological range from 800–282 Ka BP. Up until now, these specimens were attributed to *H. erectus* with no controversy (Wu and Poirier, 1995; Xing, 2012; Xing et al., 2018; Zanolli et al., 2018). We note here that the two specimens (PA 525 P_4 and PA 526 P_3) from Xichuan county, Hubei Province lack accurate stratigraphic context, but their morphological signature a priori places them close to Zhoukoudian *H. erectus* (Wu and Wu, 1982). Specifically, compared with *H. sapiens*, the Xichuan premolars display large crown size and robust roots, the foveae posterior are larger than the foveae anterior (see comparative studies by Wu and Wu (1982) and Wu and Poirier (1995)). Later studies on the dental inner structure based on micro-CT technology further acknowledged a close affinity between the Xichuan specimens and Zhoukoudian *H. erectus* (Xing et al., 2018). The second sample is mid- to late Middle Pleistocene (296–194 Ka BP) hominin specimens with no clear taxonomic attribution (here referred as *Homo* sp. from China, HSPC, N=3)., Previous studies either allocated them to post-*erectus Homo* or to archaic *H. sapiens* (Wu and Poirier, 1995). They overlap slightly in time with the HEC sample. The taxonomic status of HSPC sample needs to be further examined because a lack of diagnostic features prevents a confident taxonomic designation and their dental

morphology has not been extensively studied in a comparative context (e.g., PA1578 P_3 from Panxian Dadong, see Liu et al., 2013).

The comparative sample consists of 66 fossil and extant human premolars (Table 1). More precisely, we used microCT scans of Early Pleistocene *H. erectus* (HEJ, N=4) specimens from Sangiran, Java (Zanolli et al., 2018); late Early Pleistocene *Homo* from North Africa (HNA, N=6) (Zanolli and Mazurier, 2013); Neanderthals (NEA, N=27) derived from the sites Krapina, La Chaise (Abri Bourgeois-Delaunay) and Regourdou (NESPOS database, 2019); and recent modern humans (RMH, N=29) from Africa and Eurasia (Pan et al., 2017). The dental position and label of each specimen were provided in Supplemental Online Material (SOM) Tables S1 and S2.

As our study requires a complete external root surface model, only premolars with intact roots were selected for the comparative sample. For three Chinese *H. erectus* teeth (M3887, PA525 and PA526), minor reconstructions were conducted when the roots are lightly damaged as can be seen in Figure S1. For the entire study sample the occlusal wear ranges from stage 1 to 3 following Molnar (1971).

2.2 Micro-tomographic scanning

Ten of the eleven East Asian specimens were imaged using a 225kV μ-CT scanner at the Institute of Vertebrate Paleontology and Paleoanthropology of the CAS, Beijing, with the following parameters: 120–140 kV voltage, 100–120 mA current, angular step of 0.5° over a scan angle of 360°. The final volumes were reconstructed with an isotropic voxel size ranging from 40 to 70 μm. The fossil premolar PMU M3887 housed at Uppsala University was scanned at the Multidisciplinary Laboratory of the ICTP, Trieste (Zanolli

et al., 2018). Information on the crown outer and inner morphology were available for some specimens in previous publications (see Table 1). Root and pulp canal form of these specimens was evaluated using cross-sectional analyses (Pan and Zanolli, 2019).

A semi-automatic threshold-based segmentation was conducted using Avizo 8.0 (FEI Visualization Sciences Group,), following an adaptation of the half-maximum height method (Fajardo et al., 2002; Spoor et al., 2003; Coleman and Colbert, 2007). Cementum deposits (if any) were separated from the root dentine surface and were not included in the GM analysis. Considering that cementum helps maintain the integrity of the root grows throughout life (Selvig, 1965; Bosshardt and Selvig, 1997; Yamamoto et al., 2016), and is probably correlated with severe attrition and stress (e.g., Trinkaus et al., 2008), as distinct from dentine tissue, the removal of cementum deposit is warrented. After the segmentation, a surface model was generated using the "unconstrained smoothing" parameter in Aviso. The 3D models of the right teeth were flipped so as to for comparison with the rest of the sample.

2.3 Root metrics and statistical tests

Using Avizo 8.0, premolar root metrics were assessed using published methods (Kupczik and Dean, 2008; Kupczik and Hublin, 2010; Le Cabec et al., 2013; Moore et al., 2013; Kupczik et al., 2019). Seven variables were collected (Fig. 1 and Table 2): root length (RL, in mm, the maximum length was taken in multi-rooted teeth), root diameter (the mesio-distal as well as the bucco-lingual diameters, in mm), lateral enamel surface area (LEA, mm^2), root surface area (RA, mm^2), root volume (RV, mm^3), root pulp cavity volume (Vrpc, mm^3) and cementum volume when present (Vce, mm^3). Two indices were derived from the collected variables: the crown-root ratio (CRR=LEA/RA*100) and the ratio between bucco-lingual and

mesio-distal root diameters (D(b-l)/D(m-d)).

For separating root(s) from the crown, we defined 10–20 landmarks along the cervical line (Fig. 1) and used the "slice—points to fit" option in Aviso to generate a cervical plane (i.e., the best-fit plane of the cervical line): the crown and root(s) were then sectioned through the cervical plane (plane A). Root length is the (maximum) distance between root apex to plane A, root diameters were measured based on plane A. Root volume and the volume of the root pulp chamber were also measured based on the cervical plane (see Fig. 1 and Table 2 for detailed definition of parameters). Plane A was then moved gradually to the occlusal side of the tooth, until the most apical plane (plane B) showing the occlusal enamel was located. The enamel area between planes A and B is the lateral enamel surface area (LEA, mm^2), the root surface area from plane A to the root apex is the root area (RA, mm^2). Differences in the distribution of LEA, RA and CRR between groups were tested using the rank-based Kruskal-Wallis test with Conover's post hoc comparisons (see Table S3 for details).

2.4 Geometric morphometric analyses

We applied a recently developed geometric morphometric (GM) landmark-free approach to compare the root external surface shape (see previous applications on primate teeth in Beaudet et al., 2016; Zanolli et al., 2018). This method relies on the construction of group-average surface models and their deformation to the investigated surfaces (Durrleman et al., 2012a, b; Dumoncel et al., 2014). The surfaces are represented by a set of oriented faces and the comparison does not assume a point-to-point correspondence between samples, as in classical landmark-based GM analyses. First, the unscaled root surfaces of each tooth class were aligned together using the "Align Surface" module in Avizo 8.0. Then deformations between surfaces were mathematically modeled as a diffeomorphism, i.e., a one-to-one deformation of the 3D space that is

smooth, invertible, and with a smooth inverse, which is particularly appropriate for comparing overall shapes and local orientation in the field of computational anatomy (Glaunes and Joshi, 2006; Durrleman et al., 2014). From a set of surfaces, together with a set of initial control points located near its most variable parts, a mean shape and a set of momenta parameterizing the deformations of the mean shape to each individual were estimated (Durrleman et al., 2012a, b). Using the packages ade4 1.7-13 (Dray and Dufour, 2007) and Morpho v.2.6 (Schlager et al., 2018) for R v.3.5.1 (R Development Core Team, 2018), a between-group principal component analysis (bgPCA) (Mitteroecker and Bookstein, 2011) was performed. We first conducted principal component analysis (PCA) using deformation momenta to reduce the dimensions of our dataset, and computed the bgPCA from a subset of PCA scores (8~10) which accumulates around 90% of the overall shape variation. The three Chinese *Homo* sp. specimens were projected a posteriori in the bgPCA plot. The residual of allometric signals were tested using the coefficient of determination (R^2) of a multiple regression (Bookstein, 1991) in which the explicative variable is the root area as proxy for size and the dependent variables are the bgPC scores.

Results

3.1 Comparisons of external root morphology

Distal and lingual views of each East Asian fossil maxillary and mandibular premolar are shown in Figures 2 and 3, together with representatives of the comparative sample. Most of the East Asian Middle Pleistocene upper premolars show relatively derived features compared with East African early *Homo* (Wood et al., 1988). Whereas the latter usually appear to be double or triple-rooted, the East Asian Middle Pleistocene sample shows incompletely separated or fused buccal and lingual branches with bifid apex (Fig.

2A, C and I). This is similar to Early Pleistocene *H. erectus* from Sangiran (Fig. 2D and J) and clearly is different from bifid or single-rooted premolars generally seen in later *Homo* (recent modern humans and Neanderthals, Fig. 2E–H, K and L). Only one *H. erectus* specimen (PA 831 from Hexian) displays an early *Homo*-like condition with three well-separated root branches that spread in different directions, covered with thick cementum (Fig. 2B). The *Homo* sp. specimen PA 76 from Changyang has two nearly parallel fused branches (with thick cementum at the apex) indented by a large and deep distal groove (Fig. 2C). This P^3 configuration is similar to Indonesian *H. erectus* (Fig. 2D) and Neanderthals (Fig. 2E, F), and can be found in modern humans, but the root of PA 76 differs considerably from Chinese *H. erectus* premolars whose lingual root branch is markedly diverging (Fig. 2A and B). For the P^4s, the only *H. erectus* from China (PA 68, Zhoukoudian site) shows sub-parallel branches linked together with short free apices (Fig. 2I), but a broad generalization cannot be made on the basis of a single tooth. The pattern expressed for PA 68 (*H. erectus* from Zhoukoudian site) is not found in any other specimens. Indonesian *H. erectus* shows diverging branches at mid-root (Fig. 2J), while Neanderthals and modern humans tend to have fused roots until the apex with a deep distal groove delineating the branches (Fig. 2K, L).

With regard to lower premolars, in contrast to the North African late Early Pleistocene hominins from Tighenif that show a radical groove with two root apices (Fig. 3D, M and N), the East Asian hominins exhibit a single root with one apex (Fig. 3A–C, I–L), even if some of them also express a slight degree of Tomes' root. The East Asian fossil hominins mostly differ from later *Homo* by their more vertically oriented and pillar-like root axis, as well as a considerable amount of cementum deposit which makes them more robust than modern humans (Fig. 3D, L), while the root apex tends to be leaning more distally in the latter groups (Fig. 3E–H, O–S). It is also important to note that East Asian *H. erectus* generally show stout and large root

branches (also reported by Xing et al., 2018; Zanolli et al., 2018). As for the late Middle Pleistocene *Homo* sp., the slender root with sharp apical-third of the P_3 PA 1578 (site Panxian Dadong) (Fig. 3C) resembles the morphology found in modern humans, while the P_4 specimen PA 81 (site Changyang) (Fig. 3L) has three fused root branches, as the cementum covers 3/4 of the root body, the overall morphology of PA 81 root approximates *H. erectus* condition.

3.2 Root dimensions and volumetric measurements

HEC and HNA display the largest root volume, followed by Neanderthals and modern humans. Sangiran *H. erectus* premolars exhibit a low total root volume in P^3 that is comparable to modern humans (Fig. 4A, B; Tables S1 and S2), but Sangiran P^4s have a larger root volume, falling within the distribution of Neanderthals. The late Middle Pleistocene *Homo* sp. PA 76 P^3 (Changyang site) and PA 1578 P_3 (Panxian Dadong site) show a root volume that is in the range of both Chinese *H. erectus* and Neanderthals (Fig. 4A), , but PA 81 P_4 from Changyang exhibits a large root volume that exceeds all other lower premolars examined here (Fig. 4B).

Chinese *H. erectus* and North African *Homo* have the largest root pulp chamber volume, followed by Neanderthals. Modern humans display the smallest pulp volume among groups (Figs. 4C, D). PA 1578 P_3 and PA 81 P_4 exhibit large pulp volume, reaching (or even exceeding) the range of earlier groups like HNA and HEC (Figs. 4C, D). Root pulp chamber volume of the only Sangiran *H. erectus* specimen that we could segment falls within the range of Neanderthals (Fig. 4C), as does that of PA 76 P^3 from Changyang.

We were able to clearly segment the cementum layers in six of our eleven East Asian Middle Pleistocene specimens (Table S2). A large amount of cementum is observed in East Asian and North African fossil

hominins and some of the Neanderthal specimens (mainly from La Chaise-Abri-Bourgeois-Delaunay and Regourdou). These specimens are clearly distinct from modern humans both in the presence and volume of cementum, as easily seen on the root surface (Figs. 2 and 3). Le Cabec et al. (2013) reported an extensive degree of hypercementosis in Krapina Neanderthals. Unfortunately, the (possible) presence of a cementum layer is difficult to identify on the Krapina premolar examined here from the micro-CT scans. Due to strong fossilization, cementum deposits cannot be identified in Javanese *H. erectus* either. Further quantification of the volume as well as the 3D distribution of cementum in these specimens will require higher-quality data.

3.3 Crown-root surface area proportions

Nonparametric tests reveal significant differences in lateral enamel area (LEA) and root area (RA) among groups, but no significant differences among groups in crown root ratio (CRR). Conover's post hoc tests demonstrate distinctions between fossil and modern taxa (Table S3), but it should be pointed out that our sample size is small, statistical inferences should be addressed with caution.

For the P^3, the lowest CRR values are found in the Chinese *H. erectus* specimens PA 67 (from Zhoukoudian) and PA 832 (from Hexian) (Table 3 and Fig. 4E), suggesting a relatively large root surface area, though these are not statistically significant. It overlaps with the lower range of Neanderthals, but not with the values of Sangiran 4 and recent modern humans (Fig. 4E). The CRR of PA 76 (from Changyang) is near the average for modern humans and overlaps the Neanderthal range (Fig. 4E). Modern humans have significantly smaller absolute enamel and root surface area than Sangiran 4, early to mid-Middle Pleistocene East Asian *H. erectus* and Neanderthals (Table S3), but do not differ from the estimates of the P^3 PA 76 from Changyang. For the P^4, the Zhoukoudian *H. erectus* specimen PA 68 shows a similar signal to the P^3s, with low CRR values. With regard to mandibular premolars, marked overlap of CRR is seen between the groups

(Table 3 and Fig. 4F). Modern humans have significantly smaller root area than all the fossil groups (Table 3 and Table S3), resulting in higher crown-root proportions (Fig. 4F). One late Middle Pleistocene Chinese *Homo* sp. specimen (P_3 PA 1578 from Panxian Dadong) shows a high CRR value, even exceeding the high estimates of Neanderthals and modern humans (Fig. 4F). In contrast, the CRR ratio of the P_4 PA 81 from Changyang is considerably lower than the other groups, including the early to mid-Middle Pleistocene Chinese *H. erectus* specimens (Table 3, Fig. 4F and Table S2).

3.4 Geometric morphometric analyses

GM analysis of root shape shows substantial morphological distinctions among groups (Fig. 5). There is also an allometric signal observed along bgPC1 and/or bgPC2 for tooth positions P^3, P^4 and P_4 (Table S4), mostly distinguishing the late Early/early Middle Pleistocene specimens from North Africa and Indonesia from the Eurasian groups fossil and extant groups. *H. erectus* specimens from Sangiran and the late Early Pleistocene North African *Homo* specimens from Tighenif are distinguished morphologically from modern humans and Neanderthals along bgPC1, the former showing separated root branches while the latter mostly exhibit fused roots/single root. Regarding P^3s, recent modern humans are placed at the upper part of bgPC2 by showing separated root branches (Fig. 5A), while Neanderthals show incompletely separated roots. Two of the East Asian specimens, the Zhoukoudian *H. erectus* specimen PA 67 and the late Middle Pleistocene *Homo* sp. specimen PA 76 from Changyang site show similarities with Neanderthals, while the Hexian *H. erectus* tooth PA 832 exhibits a primitive condition with three separated root branches (Fig. 5A). The Chinese *H. erectus* specimen PA 68 falls between the ranges of of later the *Homo* groups (Fig. 5B), showing single root with bifid apex. Fused root branches separate younger hominin groups from Sangiran *H. erectus*. Regarding lower premolars, hominins from Tighenif are at the lower end of bgPC1 (Figs. 5C and D), showing

strongly expressed radical grooves at the distal or distolingual face of the root, and a tendency for separated root tips at the apex. The *H. erectus* P_3s from China (PA 110 Zhoukoudian, PA 526 Xichuan) are located at the lower half of bgPC2, indicating that they tend to have stout root body and blunt apex (Fig. 5C), in accordance with gross observation (Fig. 3E, F). In contrast, the root shape of *Homo* sp. specimen PA 1578 from Panxian Dadong falls within the modern human range and is quite distant from Neanderthals (Fig. 5C). For the lower P_4s, the *Homo* sp. specimen PA 81 from Changyang is closer to the Chinese *H. erectus* range, showing an intermediate morphology between the more archaic figure represented by the Tighenif premolars and the Neanderthal root shape (Fig. 5D).

4. Discussion

Premolar root anatomy in great apes and hominins has long been recognized to reflect taxonomy, phylogeny, and function (e.g., Wood et al., 1988; Kupczik et al., 2003; Prado-Simón et al., 2012a; Moore et al., 2016). Several studies have discovered a mosaic of primitive and derived dental traits among the so-called archaic *H. sapiens* or post-*erectus Homo* from the East Asian mid- to late Middle Pleistocene (e.g., specimens from Panxian Dadong and Changyang) (Chia, 1957; Wu and Poirier, 1995; Liu et al., 2013), but these traits are not diagnostic enough to link these specimens to any particular *Homo* species, and therefore the taxonomic assignment of these specimens remains inconclusive (Liu et al., 2013).

Recent observations on the root-canal configuration (Pan and Zanolli, 2019) as well as the qualitative and quantitative comparisons of external root morphology presented here reveal a modern-like trend of root fusion and root number reduction for the East Asian mid- to late Middle Pleistocene *Homo* sp. specimens. They differ from Chinese *H. erectus* in that the latter taxon generally shows stout premolar root(s) with thick cementum (Xing et al., 2018; Pan and Zanolli, 2019). Moreover, when multiple root branches exist, the upper

premolar roots of East Asian *H. erectus* often spread in different directions (including *H. erectus* from Yiyuan site reported by Xing et al., 2016). These features of in East Asian *H. erectus* could be interpreted as a functional response to withstand high biomechanical forces and better sustain high occlusal loads (Macho and Spears, 1999; Kupczik et al., 2005, 2018; Xing et al., 2018). In any case, the stout, pillar-like morphology of Chinese *H. erectus* premolars represent an autapomorphic feature characterizing this fossil human group (Weidenreich, 1937; Liu et al., 2017; Xing et al., 2018). The analyses presented here of root and cementum volume further confirms that larger roots and considerable cementum deposits are commonly found in East Asian *H. erectus*, late Early Pleistocene *Homo* from Tighenif and those mid- to late Middle Pleistocene hominins found in China.

4.1 Implications of root metrics and, crown-root tissue proportions

Compared with modern humans, Neanderthals have larger root and pulp volume in both the anterior (Le Cabec et al., 2013) and molar dentition (Kupczik and Hublin, 2010). Our results show that Neanderthals display larger premolar roots as well, although our sample size is small. Compared with modern humans, East Asian Middle Pleistocene hominins show larger root, pulp chamber and cementum volume. An increased root volume and pulp chamber volume may be due to a high frequency of occlusal loads. In addition, a large pulp chamber could allow for deposition of tertiary dentine (Le Cabec et al., 2012, 2013).

In hominids, root surface area is linked to masticatory function, with larger root surface area suggested to be adaptively associated with higher occlusal loads and higher mechanical resistance of food items (Kupczik et al., 2003, 2005, 2018; Spencer, 2003; Kupczik and Dean, 2008). It has been suggested that the larger molar root area in Neanderthals as compared to recent and Pleistocene *H. sapiens* could indicate that Neanderthals were able to generate larger biting forces (Kupczik and Hublin, 2010). However, a study based

on finite element analyses showed that the taurodont morphology of the Neanderthal post-canine dentition did not improve the functional biomechanics of the tooth (Benazzi et al., 2014). Thus it is still uncertain if the enlargement of premolar root area observed in Chinese *H. erectus*, together with their robust and stout premolar roots (Xing et al., 2018), reflects an adaptation to mechanically resistant diet, or to other evolutionary processes. Considering that their average premolar root area approximates that of Neanderthals, we hypothesize that it more likely represents an adaptation to a high attrition diet or is a by-product of pleiotropy or genetic drift (Benazzi et al., 2014). Future analyses based on finite element analyses will help to resolve this question.

4.2 Taxonomic and phylogenetic value of external root shape

External root shape carries a taxonomic signal, but due to the lack of homologous landmarks, 3D morphometric analysis is often limited to an broad approximation of the real root morphology (e.g., Emonet, 2009, 2012; Kupczik et al., 2018). (Semi)landmark-based GM is effective in depicting root morphology of the anterior dentition, as the surface relief of incisors and canines is relatively simple with few bifurcations or grooves (Le Cabec et al., 2013). In contrast to the above-mentioned studies, this analysis uses deformation-based GM that for the first time compares the complete premolar root surface morphology in fossil and modern humans, and explore the reliability of the radicular conformation for assessing taxonomy. Overall, there is a clear distinction between the Early Pleistocene and Late Pleistocene to Holocene human groups. The different root morphology of Neanderthals and modern humans are also clearly identified in these GM analyses. However, Chinese early Middle Pleistocene *H. erectus* premolar roots (PA 67 P^3 and PA 68 P^4, Zhoukoudian site, 800–770 Ka) tend to show a morphology that either approximates the Neanderthal condition, or that is intermediate between Neanderthals and modern humans. The late Middle Pleistocene

hominin from Changyang (PA 76 P^3) is closely placed with one East Asian *H. erectus* specimen (PA 67), and they both fall close to the range of Neanderthals. Whether this result indicates a phylogenetic link between Chinese *H. erectus* and Neanderthals (or with the still underrepresented Denisovans which shows Tomes' root in P_3, a trait that is commonly seen in fossil hominins but is also seen in modern humans (Chen et al., 2019)) or reflects homoplasy will need to be assessed in the future, integrating evidence from the crown morphology and notably from the enamel-dentine junction, which is recognized as offering significant phylogenetic information (e.g., Macchiarelli et al., 2006, 2013; Skinner et al., 2008a, b, 2009; Zanolli et al., 2014; Zanolli, 2015; Pan et al., 2016, 2017).

Considering that the fossil and modern human groups included here can be clearly distinguished by premolar morphology, we wanted to evaluate where the mid- to late Middle Pleistocene hominin specimens from China would fit. As previously mentioned, the P^3 specimen dated to the late Middle Pleistocene period from Changyang falls next to the range of Neanderthals (Fig. 5A) and shows a close affinity with one early Middle Pleistocene *H. erectus* (PA 67 from Zhoukoudian site); the mid-Middle Pleistocene P_3 (PA 1578 from Panxian Dadong), however, is clearly situated within the modern human distribution (Fig. 5C). The P_4 specimen from Changyang (PA 81) shares a similar shape with older Chinese *H. erectus* and is distinguished from the Early Pleistocene specimens from Tighenif, as well as from Neanderthals and modern humans (Fig. 5D). The root of PA 81 is quite robust, three-grooved and exhibits a thick cementum deposit (Pan and Zanolli, 2019). The absolutely large enamel and root area, large root and pulp chamber volume also point toward a *H. erectus*-like signal. We thus interpret the root structural signature of this specimen as retaining primitive features, compatible with the hypothesis that a *H. erectus*-like lineage survived in the late Middle Pleistocene. However, it should be noted that although the P^3 PA 76 from Changyang has similar root shape to Chinese

H. erectus, it has smaller pulp chamber volume and relative root surface area within the range of modern humans instead of *H. erectus*. Further analysis on other morphological aspects of this specimen is needed before a taxonomic assessment can be made with any confidence. On the other hand, the late Middle Pleistocene hominin PA 1578 from Panxian Dadong is clearly distinct from any of the Pleistocene samples and falls within the variability of modern humans. In fact, previous study on crown morphology of the four hominin teeth found at Panxian Dadong (I^1, C_1, P^3, and P_3) suggested that these teeth show a combination of archaic and modern-like features that is in line with Middle and Upper Pleistocene populations from East and West Asia (Liu et al., 2013). Our observations on the root morphology further recognize the primitive morphology of Panxian Dadong P_3 (e.g., a relatively stout root compared with modern humans, and considerable cementum covering 2/3 part or the root, Fig. 3L). On the other hand, small root and pulp chamber volume and a small relative root surface area place PA 1578 close to modern humans. We concur that this specimen likely belonged to an ancient population that is close to modern humans. Based on crown and root morphology, these "archaic *H. sapiens*" or "non-*erectus*" hominins like Panxian Dadong (Liu et al., 2013), and Tongzi (Xing et al., 2019) from the mid- to late Middle Pleistocene and the Xujiayao hominin from the early Late Pleistocene (Xing et al., 2015) express remarkable derived features that is typically found in later *Homo* lineages. The dispersal of these "non-*H. erectus*" hominins might be further clarified following a comparative study on the dentition of the Denisovan specimen from the Xiahe site (Chen et al., 2019). Moreover, it is important to underscore that there is root shape variation in the East Asian *H. erectus* sample: for instance, robust and fully separated root branches are found in PA 832 P^3, a mid-Middle Pleistocene *H. erectus* from Hexian site, while the older PA 67 P^3 from Zhoukoudian shows incompletely separated double roots (also see Pan and Zanolli, 2019). This may indicate a late survival of archaic lineages, which is in line

with previous studies on crown morphology (Xing et al., 2014; Liu et al., 2017).

Previous investigations of hominin dental crown morphology using GM techniques (Martinón-Torres et al., 2006; Gómez-Robles et al., 2007, 2008) have observed different evolutionary trends in different dental positionswithin the same tooth class. For example, Neanderthals show a primitive P_4 morphology but a derived P_3. Furthermore, morphogenesis of the upper and lower dentition are under the control of different genetic programs (Thomas et al., 1997; McCollum and Sharpe, 2001). Given this, we emphasize that any taxonomic interpretation of our results must be approached with caution and placed within a larger context—especially with the incorporation of other dental morphological evidence. Nonetheless, our preliminary results show that in contrast to non-metric configurations (e.g., root number and form (Abbott, 1984; Wood et al., 1988; Moore et al., 2015; Moore et al., 2016)) and standard metrics (e.g., root length and width (Kupczik and Hublin, 2010; Prado-Simón et al., 2012b; Le Cabec et al., 2013)), GM analysis of premolar root surface is an useful indicator for taxonomy. On the other hand, we caution that other than root length and some particular metrics that distinguish the roots of modern humans vs. Neanderthals (e.g., Le Cabec et al., 2012, 2013), root shape and structure are highly phenotypically plastic and quite variable within groups. Recent studies have demonstrated that there is considerable variation in premolar root number within a single species, and even in the same individual (Kupczik et al., 2005; Shields, 2005; Moore et al., 2015, 2016). However, as shown in our GM analyses, despite differences in root shape, it is still possible to quantify differences between recent humans and Pleistocene human groups/taxa and separate them.

5. Conclusion

This study first provides a quantitative comparison of permanent maxillary and mandibular premolar root morphologies in Chinese Middle Pleistocene hominins. Stout root shape, relatively large root area, large

root and pulp chamber volume and a considerable amount of cementum deposit are commonly observed in East Asian Middle Pleistocene *H. erectus* (Xing et al., 2018; this study). Together with previous landmark-based GM studies on hominoid molars (Emonet et al., 2012), the present work suggests that external root surface morphology is taxonomically informative. The 3D landmark-free approach to quantify dental root surface morphology in fossil and modern humans, and used here is able to discriminate among several hominin groups, and enabled evaluation of the taxonomic affinities of a number of East Asian Middle Pleistocene hominin specimens. Integration of a larger sample and other dental evidence from more diverse time periods localities should help to better characterize the spatial-temporal dispersal of multiple *Homo* lineages in East Asia. In addition, as molar root form is more conservative in its phenotypic expression, further study on molar root surface morphology may also provide useful information on the evolutionary relationships in fossil hominins.

Crown-root metrics (lateral enamel area, root area and crown-root ratio) together with external root GM analyses suggest that among the three Chinese mid- to late Middle Pleistocene *Homo* sp. specimens investigated here, the two premolars from Changyang (the P^3 PA 76 and the P_4 PA 81) retain some primitive features in their root structure and are possibly late representatives of a *H. erectus*-like lineage. Conversely, the third specimen (P_3 PA 1578 from Panxian Dadong) exhibits unambiguous modern-like features and may represent evidence for an early presence of modern humans in Asia. In addition, recent study on the 240–172 Ka dental remains from Tongzi site, China hints at the existence of multiple paleodemes in East Asian during mid- to late Middle Pleistocene period (Xing et al., 2019). Even if the available dating ranges of these specimens do not fully overlap, the penecontemporaneity of the Changyang and Panxian Dadong hominins is reasonable, suggesting that our results are potentially consistent with the possible coexistence of multiple

human lineages in East Asia during the late Middle Pleistocene.

References

Abbott, S.A., 1984. A comparative study of tooth root morphology in the great apes, modern man and early hominids. Ph. D. Dissertation, University of London.

An, Z.S., Kun, H.C., 1989. New magnetostratigraphic dates of Lantian *Homo erectus*. Quaternary Research 32, 213–221.

Bailey, S.E., Liu, W., 2010. A comparative dental metrical and morphological analysis of a Middle Pleistocene hominin maxilla from Chaoxian (Chaohu), China. Quaternary International 211, 14–23.

Beaudet, A., Dumoncel, J., Thackeray, F., Bruxelles, L., Duployer, B., Tenailleau, C., Bam, L., Hoffman, J., de Beer, F., Braga, J., 2016. Upper third molar internal structural organization and semicircular canal morphology in Plio-Pleistocene South African cercopithecoids. Journal of Human Evolution 95, 104–120.

Benazzi, S., Nguyen, H.N., Kullmer, O., Hublin, J.-J., 2014. Exploring the biomechanics of taurodontism. Journal of Anatomy 226, 180–188.

Bookstein, F., 1991. Morphometric Tools for Landmark Data: Geometry and Biology. Cambridge University Press, Cambridge.

Bosshardt, D.D., Selvig, K.A., 1997. Dental cementum: the dynamic tissue covering of the root. Periodontology 2000 13, 41–75.

Braga, J., Zimmer, V., Dumoncel, J., Samir, C., de Beer, F., Zanolli, C., Pinto, D., Rohlf, F.J., Grine, F.E., 2019. Efficacy of diffeomorphic surface matching and 3D geometric morphometrics for taxonomic discrimination of Early Pleistocene hominin mandibular molars. Journal of Human Evolution 130, 21–35.

Chen, F., Welker, F., Shen, C.-C., Bailey, S.E., Bergmann, I., Davis, S., Xia, H., Wang, H., Fischer, R., Freidline, S.E., 2019. A late Middle Pleistocene Denisovan mandible from the Tibetan Plateau. Nature 569,

409.

Chia, L., 1957. Notes on the human and some other mammalian remains from Changyang, Hupei. Vertabrata Palasiatica 1, 179–190.

Coleman, M.N., Colbert, M.W., 2007. CT thresholding protocols for taking measurements on three-dimensional models. American Journal of Physical Anthropology 133, 723–725.

Dou, L., Li, D., Xu, T., Tang, Y., Yang, D., 2017. Root anatomy and canal morphology of mandibular first premolars in a Chinese population. Scientific Reports 7, 750.

Dray, S., Dufour, A.-B., 2007. The ade4 package: implementing the duality diagram for ecologists. Journal of statistical software 22, 1–20.

Dumoncel, J., Durrleman, S., Braga, J., Jessel, J.-P., Subsol, G., 2014. Landmark-free 3D method for comparison of fossil hominins and hominids based on endocranium and EDJ shapes. American Journal of Physical Anthropology 153, suppl. 56, 110.

Durrleman, S., Pennec, X., Trouvé, A., Ayache, N., Braga, J., 2012a. Comparison of the endocranial ontogenies between chimpanzees and bonobos via temporal regression and spatiotemporal registration. Journal of Human Evolution 62, 74–88.

Durrleman, S., Prastawa, M., Korenberg, J.R., Joshi, S., Trouvé, A., Gerig, G., 2012b. Topology preserving atlas construction from shape data without correspondence using sparse parameters. In: Ayache, N., Delingette, H., Golland, P., Mori, K. (Eds.), Proceedings of Medical Image Computing and Computer Assisted Intervention. Nice, France, pp. 223–230

Durrleman, S., Prastawa, M., Charon, N., Korenberg, J.R., Joshi, S., Gerig, G., Trouvé, A., 2014. Morphometry of anatomical shape complexes with dense deformations and sparse parameters. NeuroImage 101, 35–49.

Emonet, E.-G., 2009. *Khoratpithecus* et la radiation des hominoïdes en Asie du Sud-Est au Miocène. Ph. D. Dissertation, Université de Poitiers.

Emonet, E.-G., Tafforeau, P., Chaimanee, Y., Guy, F., De Bonis, L., Koufos, G., Jaeger, J.-J., 2012. Three-dimensional analysis of mandibular dental root morphology in hominoids. Journal of Human Evolution 62, 146–154.

Emonet, E.G., Andossa, L., Taïsso Mackaye, H., Brunet, M., 2014. Subocclusal dental morphology of *Sahelanthropus tchadensis* and the evolution of teeth in hominins. American Journal of Physical Anthropology 153, 116–123.

Fajardo, R.J., Ryan, T., Kappelman, J., 2002. Assessing the accuracy of high-resolution X-ray computed tomography of primate trabecular bone by comparisons with histological sections. American Journal of Physical Anthropology 118, 1–10.

Glaunes, J.A., Joshi, S., 2006. Template estimation form unlabeled point set data and surfaces for computational anatomy. In: Pennec, X., Joshi, S. (Eds.), 1st MICCAI Workshop on Mathematical Foundations of Computational Anatomy: Geometrical, Statistical and Registration Methods for Modeling Biological Shape Variability. Copenhagen, Denmark, pp. 29–39

Gómez-Robles, A., Martinón-Torres, M., Bermúdez de Castro, J.M., Margvelashvili, A., Bastir, M., Arsuaga, J.L., Pérez-Pérez, A., Estebaranz, F., Martínez, L.M., 2007. A geometric morphometric analysis of hominin upper first molar shape. Journal of Human Evolution 53, 272–285.

Gómez-Robles, A., Martinón-Torres, M., Bermúdez de Castro, J.M., Prado, L., Sarmiento, S., Arsuaga, J.L., 2008. Geometric morphometric analysis of the crown morphology of the lower first premolar of hominins, with special attention to Pleistocene *Homo*. Journal of Human Evolution 55, 627–638.

Grün, R., Huang, P.-H., Wu, X., Stringer, C.B., Thorne, A.G., McCulloch, M., 1997. ESR analysis of teeth from the palaeoanthropological site of Zhoukoudian, China. Journal of Human Evolution 32, 83–91.

Grün, R., Huang, P.-H., Huang, W., McDermott, F., Thorne, A., Stringer, C.B., Yan, G., 1998. ESR and U-series analyses of teeth from the palaeoanthropological site of Hexian, Anhui Province, China. Journal of Human Evolution 34, 555–564.

Huang, P.-H., Jin, S.-Z., Peng, Z.-C., Liang, R.-Y., Lu, Z.-J., Wang, Z.-R., Chen, J.-B., Yuan, Z.-X., 1993. ESR dating of tooth enamel: comparison with U-Series, FT and TL dating at the Peking Man Site. Applied Radiation and Isotopes 44, 239–242.

Huffman, O.F., 2001. Geologic context and age of the Perning/Mojokerto *Homo erectus*, East Java. Journal of Human Evolution 40, 353–362.

Kaifu, Y., Baba, H., Aziz, F., Indriati, E., Schrenk, F., Jacob, T., 2005. Taxonomic affinities and evolutionary

history of the Early Pleistocene hominids of Java: dentognathic evidence. American Journal of Physical Anthropology 128, 709–726.

Kaifu, Y., Kono, R.T., Sutikna, T., Saptomo, E.W., Jatmiko, Awe, R.D., Baba, H., 2015. Descriptions of the dental remains of *Homo floresiensis*. Anthropological Science 123, 129–145.

Karkanas, P., Schepartz, L.A., Miller-Antonio, S., Wang, W., Huang, W., 2008. Late Middle Pleistocene climate in southwestern China: inferences from the stratigraphic record of Panxian Dadong Cave, Guizhou. Quaternary Science Reviews 27, 1555–1570.

Kupczik, K., Spoor, F., Dean, M.C., 2003. Tooth root morphology and masticatory muscle force pattern in humans and nonhuman primates. American Journal of Physical Anthropolology Supplement 36, 134.

Kupczik, K., Spoor, F., Pommert, A., Dean, M.C., 2005. Premolar root number variation in hominoids: genetic polymorphism vs. functional significance, In: Żądzińska E (Ed.), Current Trends in Dental Morphology Research. University of Lodz Press, Lodz, pp. 257–268.

Kupczik, K., Dean, M.C., 2008. Comparative observations on the tooth root morphology of *Gigantopithecus blacki*. Journal of Human Evolution 54, 196–204.

Kupczik, K., Olejniczak, A.J., Skinner, M.M., Hublin, J.-J., 2009. Molar crown and root size relationship in anthropoid primates. Frontiers in Oral Biology 13, 16–22.

Kupczik, K., Hublin, J.-J., 2010. Mandibular molar root morphology in Neanderthals and Late Pleistocene and recent *Homo sapiens*. Journal of Human Evolution 59, 525–541.

Kupczik, K., Toro-Ibacache, V., Macho, G.A., 2018. On the relationship between maxillary molar root shape and jaw kinematics in *Australopithecus africanus* and *Paranthropus robustus*. Royal Society Open Science 5, 180825.

Kupczik, K., Delezene, L.K., Skinner, M.M., 2019. Mandibular molar root and pulp cavity morphology in *Homo naledi* and other Plio-Pleistocene hominins. Journal of Human Evolution 130, 83–95.

Le Cabec, A., Kupczik, K., Gunz, P., Braga, J., Hublin, J.-J., 2012. Long anterior mandibular tooth roots in Neanderthals are not the result of their large jaws. Journal of Human Evolution 63, 667–681.

Le Cabec, A., Gunz, P., Kupczik, K., Braga, J., Hublin, J.-J., 2013. Anterior tooth root morphology and size in Neanderthals: Taxonomic and functional implications. Journal of Human Evolution 64, 169–193.

Liu, W., Schepartz, L.A., Xing, S., Miller-Antonio, S., Wu, X., Trinkaus, E., Martinón-Torres, M., 2013. Late Middle Pleistocene hominin teeth from Panxian Dadong, South China. Journal of Human Evolution 64, 337–355.

Liu, W., Martinón-Torres, M., Kaifu, Y., Wu, X., Kono, R., Chang, C.-H., Wei, P., Xing, S., Huang, W., Bermúdez de Castro, J.M., 2017. A mandible from the Middle Pleistocene Hexian site and its significance in relation to the variability of Asian *Homo erectus*. American Journal of Physical Anthropology 162, 715–731.

Loh, H., 1998. Root morphology of the maxillary first premolar in Singaporeans. Australian Dental Journal 43, 399–402.

Macchiarelli, R., Bondioli, L., Debénath, A., Mazurier, A., Tournepiche, J.-F., Birch, W., Dean, C., 2006. How Neanderthal molar teeth grew. Nature 444, 748–751.

Macchiarelli, R., Bayle, P., Bondioli, L., Mazurier, A., Zanolli, C., 2013. From outer to inner structural morphology in dental anthropology: integration of the third dimension in the visualization and quantitative analysis of fossil remains, In: Scott, G.R., Irish, J. (Eds.), Anthropological perspectives on tooth morphology: Genetics, evolution, variation. Cambridge University Press, Cambridge, pp. 250-277.

Macho, G.A., Spears, I.R., 1999. Effects of loading on the biochemical behavior of molars of *Homo*, *Pan*, and *Pongo*. American Journal of Physical Anthropology 109, 211–227.

Martinón-Torres, M., Bastir, M., De Castro, J.B., Gómez, A., Sarmiento, S., Muela, A., Arsuaga, J., 2006. Hominin lower second premolar morphology: evolutionary inferences through geometric morphometric analysis. Journal of Human Evolution 50, 523–533.

Martinón-Torres, M., Bermúdez de Castro, J.M., Gómez-Robles, A., Arsuaga, J.L., Carbonell, E., Lordkipanidze, D., Manzi, G., Margvelashvili, A., 2007. Dental evidence on the hominin dispersals during the Pleistocene. Proceedings of the National Academy of Sciences 104, 13279–13282.

Martinón-Torres, M., Xing, S., Liu, W., Bermúdez de Castro, J.M., 2018. A “source and sink” model for East Asia? Preliminary approach through the dental evidence. Comptes Rendus Palevol, 33–43.

McCollum, M.A., Sharpe, P.T., 2001. Developmental genetics and early hominid craniodental evolution. BioEssays 23, 481-493.

Moggi-Cecchi, J., Menter, C., Boccone, S., Keyser, A., 2010. Early hominin dental remains from the Plio-

Pleistocene site of Drimolen, South Africa. Journal of Human Evolution 58, 374–405.

Molnar, S., 1971. Human tooth wear, tooth function and cultural variability. American Journal of Physical Anthropology 34, 175–189.

Moore, N.C., Skinner, M.M., Hublin, J.J., 2013. Premolar root morphology and metric variation in *Pan troglodytes verus*. American Journal of Physical Anthropology 150, 632–646.

Moore, N.C., Hublin, J.J., Skinner, M.M., 2015. Premolar root and canal variation in extant non-human hominoidea. American Journal of Physical Anthropology 158, 209–226.

Moore, N.C., Thackeray, J.F., Hublin, J.-J., Skinner, M.M., 2016. Premolar root and canal variation in South African Plio-Pleistocene specimens attributed to *Australopithecus africanus* and *Paranthropus robustus*. Journal of Human Evolution 93, 46–62.

NESPOS database, 2019, NEanderthal Studies Professional Online Service.

Pan, L., Dumoncel, J., de Beer, F., Hoffman, J., Thackeray, J.F., Duployer, B., Tenailleau, C., Braga, J., 2016. Further morphological evidence on South African earliest *Homo* lower postcanine dentition: enamel thickness and enamel dentine junction. Journal of Human Evolution 96, 82–96.

Pan, L., Thackeray, J.F., Dumoncel, J., Zanolli, C., Oettlé, A., De Beer, F., Hoffman, J., Duployer, B., Tenailleau, C., Braga, J., 2017. Intra-individual metameric variation expressed at the enamel-dentine junction of lower post-canine dentition of South African fossil hominins and modern humans. American Journal of Physical Anthropology 163, 806–815.

Pan, L., Zanolli, C., 2019. Comparative observations on the premolar root and pulp canal configurations of Middle Pleistocene *Homo* in China. American Journal of Physical Anthropology 168, 637–646.

Prado-Simón, L., Martinón-Torres, M., Baca, P., Olejniczak, A.J., Gómez‐Robles, A., Lapresa, M., Luis Arsuaga, J., Bermúdez de Castro, J.M., 2012a. Three-dimensional evaluation of root canal morphology in lower second premolars of early and middle pleistocene human populations from Atapuerca (Burgos, Spain). American Journal of Physical Anthropology 147, 452–461.

Prado-Simón, L., Martinón-Torres, M., Baca, P., Gómez-Robles, A., Lapresa, M., Carbonell, E., Bermúdez de Castro, J.M., 2012b. A morphological study of the tooth roots of the Sima del Elefante mandible (Atapuerca, Spain): a new classification of the teeth—biological and methodological considerations.

Anthropological Science 120, 61–72.

Radovčić, J., Smith, F.H., Trinkaus, E., Wolpoff, M.H., 1988. The Krapina Hominids: An Illustrated Catalog of Skeletal Collection. Mladost and the Croatian Natural History Museum, Zagreb.

Rink, W.J., Schwarcz, H.P., Smith, F.H., Radovčić, J., 1995. ESR dates for Krapina hominids. Nature 378, 24.

Sahnouni, M., Van der Made, J., 2009. The Oldowan in North Africa within a biochronological framework, In: Schick, K., Toth, N. (Eds.), New Approaches to the Archaeology of Human Origins. Stone Age Institute Press Bloomington, pp. 179–209.

Schlager, S., Profico, A., Di Vincenzo, F., Manzi, G., 2018. Retrodeformation of fossil specimens based on 3D bilateral semi-landmarks: Implementation in the R package "Morpho". PLOS ONE 13, e0194073.

Scott, G.R., Turner II, C.G., Townsend, G., Martinón-Torres, M., 2018. The Anthropology of Modern Human Teeth. Dental Morphology and its Variation in Recent and Fossil *Homo sapiens*. Cambridge University Press, Cambridge.

Selvig, K.A., 1965. The fine structure of human cementum. Acta Odontologica Scandinavica 23, 423–441.

Sert, S., Bayirli, G.S., 2004. Evaluation of the root canal configurations of the mandibular and maxillary permanent teeth by gender in the Turkish population. Journal of Endodontics 30, 391–398.

Shen, G., Ku, T.-L., Cheng, H., Edwards, R.L., Yuan, Z., Wang, Q., 2001. High-precision U-series dating of Locality 1 at Zhoukoudian, China. Journal of Human Evolution 41, 679–688.

Shields, E.D., 2005. Mandibular premolar and second molar root morphological variation in modern humans: what root number can tell us about tooth morphogenesis. American Journal of Physical Anthropology 128, 299–311.

Skinner, M.M., Wood, B.A., Boesch, C., Olejniczak, A.J., Rosas, A., Smith, T.M., Hublin, J.-J., 2008a. Dental trait expression at the enamel-dentine junction of lower molars in extant and fossil hominoids. Journal of Human Evolution 54, 173–186.

Skinner, M.M., Gunz, P., Wood, B.A., Hublin, J.-J., 2008b. Enamel-dentine junction (EDJ) morphology distinguishes the lower molars of *Australopithecus africanus* and *Paranthropus robustus*. Journal of Human Evolution 55, 979–988.

Skinner, M.M., Gunz, P., Wood, B.A., Boesch, C., Hublin, J.J., 2009. Discrimination of extant *Pan* species and subspecies using the enamel–dentine junction morphology of lower molars. American Journal of Physical Anthropology 140, 234–243.

Spencer, M.A., 2003. Tooth-root form and function in platyrrhine seed-eaters. American Journal of Physical Anthropology 122, 325–335.

Sperber, G.H., 1974. Morphology of the cheek teeth of early South African hominids. Ph. D. Dissertation, University of the Witwatersrand.

Spoor, F., Hublin, J.-J., Braun, M., Zonneveld, F., 2003. The bony labyrinth of Neanderthals. Journal of Human Evolution 44, 141–165.

Thomas, B.L., Tucker, A.S., Qui, M., Ferguson, C.A., Hardcastle, Z., Rubenstein, J., Sharpe, P.T., 1997. Role of Dlx-1 and Dlx-2 genes in patterning of the murine dentition. Development 124, 4811 ‐ 4818.

Tomes, C.S., 1923. A manual of dental anatomy: human and comparative. 8th ed. MacMillan Co., New York.

Trinkaus, E., Maley, B., Buzhilova, A.P., 2008. Brief communication: Paleopathology of the Kiik ‐ Koba 1 Neandertal. American Journal of Physical Anthropology 137, 106–112.

Turner, C.G., 1981. Root number determination in maxillary first premolars for modern human populations. American Journal of Physical Anthropology 54, 59–62.

Turq, A., Jaubert, J., Maureille, B., Laville, D., 2008. Le cas des sépultures néandertaliennes du Sud-Ouest: et si on les vieillissait?, In: Vandermeersch, B., Cleyet-Merle, J.-J., Maureille, B., Turq, A. (Eds.), Première Humanité, Gestes Funéraires des Néandertaliens. Réunion des Musées Nationaux, Paris, pp. 40–41.

Weidenreich, F., 1937. The dentition of *Sinanthropus pekinensis*: a comparative odontography of the hominids. Palaeontol. Sin. Series D I, 1–180.

White, T.D., Suwa, G., Simpson, S., Asfaw, B., 2000. Jaws and teeth of *Australopithecus afarensis* from Maka, Middle Awash, Ethiopia. American Journal of Physical Anthropology 111, 45–68.

Woo, J.-k., 1964. Mandible of *Sinanthropus lantianensis*. Current Anthropology 5, 98–101.

Wood, B., Engleman, C., 1988. Analysis of the dental morphology of Plio-Pleistocene hominids. V. Maxillary postcanine tooth morphology. Journal of Anatomy 161, 1–35.

Wood, B., Abbott, S., Uytterschaut, H., 1988. Analysis of the dental morphology of Plio-Pleistocene

hominids. IV. Mandibular postcanine root morphology. Journal of Anatomy 156, 107–139.

Wu, X., Wu, R., 1982. Human fossil teeth from Xichuan, Henan (In Chinese with English abstract). Vertabrata Palasiatica 20, 1–10.

Wu, X., Poirier, F.E., 1995. Human evolution in China: a metric description of the fossils and a review of the sites. Oxford University Press, New York.

Xing, S., 2012. Morphological variation of Zhoukoudian *H. erectus* teeth. Ph.D. Dissertation, Graduate University of Chinese Academy of Sciences.

Xing, S., Martinón-Torres, M., Bermúdez de Castro, J.M., Zhang, Y., Fan, X., Zheng, L., Huang, W., Liu, W., 2014. Middle Pleistocene hominin teeth from Longtan Cave, Hexian, China. PLOS ONE 9, e114265.

Xing, S., Martinón‐Torres, M., Bermúdez de Castro, J.M., Wu, X., Liu, W., 2015. Hominin teeth from the early Late Pleistocene site of Xujiayao, Northern China. American Journal of Physical Anthropology 156, 224–240.

Xing, S., Sun, C., Martinón-Torres, M., Bermúdez de Castro, J.M., Han, F., Zhang, Y., Liu, W., 2016. Hominin teeth from the Middle Pleistocene site of Yiyuan, Eastern China. Journal of Human Evolution 95, 33–54.

Xing, S., Martinón-Torres, M., Bermúdez de Castro, J.M., 2018. The fossil teeth of the Peking Man. Scientific Reports 8, 1–11.

Xing, S., Martinón-Torres, M., Bermúdez de Castro, J.M., 2019. Late Middle Pleistocene hominin teeth from Tongzi, southern China. Journal of Human Evolution 130, 96–108.

Yamamoto, T., Hasegawa, T., Yamamoto, T., Hongo, H., Amizuka, N., 2016. Histology of human cementum: Its structure, function, and development. Japanese Dental Science Review 52, 63–74.

Yuan, S., Chen, T., Gao, S., 1986. Uranium series chronological sequence of some palaeolithic sites in South China (In Chinese with English abstract). Acta Anthropologica Sinica 2, 179–190.

Zanolli, C., Mazurier, A., 2013. Endostructural characterization of the *H. heidelbergensis* dental remains from the early Middle Pleistocene site of Tighenif, Algeria. Comptes Rendus Palevol 12, 293–304.

Zanolli, C., Bondioli, L., Coppa, A., Dean, C.M., Bayle, P., Candilio, F., Capuani, S., Dreossi, D., Fiore, I., Frayer, D.W., 2014. The late Early Pleistocene human dental remains from Uadi Aalad and Mulhuli-Amo

(Buia), Eritrean Danakil: macromorphology and microstructure. Journal of Human Evolution 74, 96–113.

Zanolli, C., 2015. Brief communication: molar crown inner structural organization in Javanese *Homo erectus*. American Journal of Physical Anthropology 156, 148–157.

Zanolli, C., Pan, L., Dumoncel, J., Kullmer, O., Kundrát, M., Liu, W., Macchiarelli, R., Mancini, L., Schrenk, F., Tuniz, C., 2018. Inner tooth morphology of *Homo erectus* from Zhoukoudian. New evidence from an old collection housed at Uppsala University, Sweden. Journal of Human Evolution 116, 1–13.

Table 1. Composition of the study sample

Specimen	P^3	P^4	P_3	P_4	Provenance	Chronological range [a]	Citations [b]
Middle Pleistocene *H. erectus* from China (HEC)							
PA 102				1	Chenjiawo	650–500 Ka (A)	1
PA 110			1		Layer 3	320–282 Ka (B, C) 500 Ka (D)	2, 3
PMU M3887 [c]				1	Zhoukoudian Loc. 1 Layer 5	550–500 Ka (E)	4, 5
PA 67	1				Layer 11	800–770 Ka (F)	2, 3
PA 68		1					
PA 832	1				Hexian	437–387 Ka (E)	6, 7
PA 525 [c]				1	Xichuan	Unknown	8
PA 526 [c]			1				
Late Middle Pleistocene *Homo sp.* from China (HSPC)							
PA 76	1				Changyang	196–194 Ka (F)	9
PA 81				1			
PA 1578			1		Panxian Dadong	296–233 Ka (G)	10
Early Pleistocene *H. erectus* (HEJ)							
Sangiran 4	2	2			Pucangan Fm. **Sangiran**	1.8–1.6 Ma (H)	5
Early Pleistocene *Homo* from North Africa (HNA)							

Tighenif 1			2	2	Tighenif		~1.0 Ma (I)	11
Tighenif 2			1	1				
	3	7	4	5	Level 8	**Krapina**	140–120 Ka (J)	12, 13
Neanderthals (NEA)		1	2	1	Abri Bourgeois–Delaunay	La Chaise	146–106 Ka (K)	13, 14
			2	2		**Regourdou**	70 Ka (L)	13
Recent Modern Humans (RMH)	5	7	8	9	Asian/ European/ South African			15

[a] Age : (A) An and Kun (1989); (B) Grün et al. (1997); (C) Huang et al. (1993); (D) Shen et al. (2001); (E) Grün et al. (1998); (F) Yuan et al. (1986); (G) Karkanas et al. (2008); (H) Huffman (2001); (I) Sahnouni and Van der Made (2009); (J) Rink et al. (1995); (K) Macchiarelli et al. (2006) ; (L) Turq et al. (2008)

[b] Citations: (1) Woo (1964); (2) Xing (2012); (3) Xing et al. (2018); (4) Black et al. (1933); (5) Zanolli et al. (2018); (6) Xing et al. (2014); (7) Liu et al. (2017); (8) Bailey and Liu (2010); (9) Chia (1957); (10) Liu et al. (2013); (11) Zanolli and Mazurier (2013); (12) Radovčić et al. (1988); (13) NESPOS database (2019); (14) Macchiarelli et al. (2006) ; (15) Pan et al. (2017)

[c] Partly damaged root, restored. For the restoration see Figure S1.

Table 2. Definition of metrics taken for the study. Protocols proposed by Kupczik and Dean (2008); Prado-Simón et al. (2012); Le Cabec et al. (2013).

Metrics	Acronym	Complete definition	Dimension	Descriptive statistics
Root length	RL	Along the long axis of the root, linear distance between the root apex and the center of the cervical plane, when more than one root branches exist, the maximum length was taken.	mm	Table S1 and Figure S2
Bucco-lingual root diameter	D(b-l)	At the cervical plane, the largest diameter of the root along the bucco-lingual direction.	mm	Table S1
Mesio-distal root diameter	D(m-d)	At the cervical plane, the largest diameter of the root along the mesio-distal direction.	mm	Table S1
Root area	RA	The total root surface area from the cervical plane to the apex.	mm^2	Table 3 and Table S2
Lateral enamel surface area	LEA	The outer enamel surface area between the cervical plane and the most apical plane (i.e., Plane B) showing the occlusal enamel that is parallel to the cervical	mm^2	Table 3 and Table S2

		plane.		
Root volume	RV	Volume of the dentine, pulp chamber and cementum in the root, between the cervical plane and the root apex.		Figure 4 andTable S2
Root pulp cavity volume	Vrpc	The volume of the pulp chamber in the root, between the cervical plane to the pulp chamber apex.	mm^3	Figure 4 and Table S2
Cementum volume	Vce	The total volume of the cementum.	mm^3	Table S2
	D(b-l)/D(m-d)	Ratio between bucco-lingual and mesio-distal root diameters.	Dimensionless	Table S1
The crown-root ratio	CRR= LEA/RA*100	Ratio between lateral enamel area and root area.	Dimensionless	Figure 4, Table 3 and Table S2

Table 3. Average values for the lateral enamel area (LEA), root area (RA) and crown-root ratio (CRR) measured in the later Middle Pleistocene *Homo sp.* from China, together with comparative samples.

Dental positions	Groups	LEA (mm^2)	RA (mm^2)	CRR (%)
P^3	HEC	80.17±3.53 [77.68 – 82.67]	453.92±64.13 [408.58–499.27]	17.78±1.73 [16.56–19.01]
	HSPC (PA 76)	86.50	335.91	25.75
	HEJ	119.98±7.61 [114.60 – 125.36]	449.39±10.78 [441.77–457.02]	26.68±1.05 [25.94–27.43]
	NEA	104.87±5.64 [100.18–111.13]	466.56±88.26 [400.25–566.74]	23.11±5.09 [17.68–27.76]
	RMH	77.91±10.41 [66.41–89.92]	295.33±46.65 [263.25–377.44]	26.54±2.51 [23.06–28.81]
	HEC (PA 68)	86.39	419.79	20.58
	HEJ	120.46±0.05 [120.43–120.50]	479.70±86.47 [418.56–540.85]	25.53±4.59 [22.28–28.77]
P^4	NEA	95.76±10.72 [80.04–113.00]	438.67±80.22 [353.97–540.00]	22.20±3.03 [17.78–27.15]
	RMH	76.40±10.81 [64.31–90.02]	289.28±36.16 [224.40–336.40]	26.52±2.88 [21.04–29.58]
P_3	HEC	76.84±4.25 [73.04–	360.71±29.57 [331.15–	21.38±1.30 [20.46–22.30]

		79.85]	390.28]	
	HSPC (PA 1578)	93.60	336.72	27.80
	HNA	77.90±7.83 [68.94–83.42]	391.95±31.16 [331.15–390.28]	20.06±3.48 [16.21–22.99]
	NEA	75.37±15.60 [56.34–103.82]	327.92±62.69 [260.64–386.01]	23.02±3.75 [17.12–26.90]
	RMH	64.46±13.25 [49.16–86.08]	261.65±64.19 [206.66–335.04]	24.61±1.72 [21.24–26.87]
	HEC	92.10±37.06 [65.89–134.50]	353.65±49.76 [295.68–395.20]	25.61±7.35 [20.51–26.51]
	HSPC (PA 81)	81.38	422.37	19.27
	HNA	111.60±8.62 [103.30–120.50]	456.60±10.60 [447.00–468.20]	24.47±2.24 [22.06–26.51]
P_4	NEA	86.16±18.50 [60.87–110.60]	330.04±65.06 [261.08–391.20]	26.16±4.86 [19.32–32.80]
	RMH	73.81±6.84 [60.46–82.44]	267.71±38.39 [224.20–300.98]	27.78±2.36 [25.24–33.21]

Abbreviations as follows: HEJ: Javanese *H. erectus*; HEC: Middle Pleistocene *H. erectus* from China; HSPC: late Middle Pleistocene *Homo sp.* from China; HNA: Early Pleistocene *Homo* from North Africa; NEA: Neanderthals; RMH: Recent modern humans. Data was reported in the form mean value ± SD [minimum–maximum].

Figure captions:

Figure 1. Lingual view of a lower premolar, illustrating the separation of the crown and root along the cervical plane, and the extraction of lateral enamel (A). Linear and volumetric measurements were taken on root(s) (B), cementum (C) and root pulp cavity (D).

Figure 2. Comparisons of external root morphology in upper premolars (cementum shown as transparent). HEC: early to mid-Middle Pleistocene *H. erectus* from China; HSPC: late Middle Pleistocene *Homo* sp. from China; HEJ: Javanese *H. erectus*; NEA: Neanderthals; RMH: recent modern humans; D: distal view; L: lingual view. Neanderthal specimen IDs were detailed in Figures S1 and S2.

Figure 3. Comparisons of external root morphology in lower premolars (cementum shown in transparent). HEC: early to mid-Middle Pleistocene *H. erectus* from China; HSPC: late Middle Pleistocene *Homo* sp. from China. HNA: Early Pleistocene *Homo* from North Africa; NEA: Neanderthals; RMH: recent modern humans; D: distal view; L: lingual view. Neanderthal specimen IDs were detailed in Figures S1 and S2.

Figure 4. Standard box and whisker plot of the root volume (A-B) and root pulp volume (C-D) and crown-root area ratio (E-F) in each group with regard to dental position, mid- to late Middle Pleistocene *Homo* sp. specimens were highlighted. A, C and E: upper premolars; B, D and F: lower premolars. The interquartile range (25^{th}-75^{th} percentiles: boxes), 1.5 interquartile ranges (whiskers) and the median values (black line) are shown. Outliers more than 1.5 interquartile ranges from the box are signified with circles, extremes more than 3 interquartile ranges from the box are signified with asterisks. Abbreviations: RV: root volume; Vrpc: root pulp chamber volume; CRR: crown-root ratio; HEJ: Javanese *H. erectus*; HEC: *H. erectus* from China; HSPC: *Homo* sp. from China; HNA: Early Pleistocene *Homo* from North Africa; NEA: Neanderthals; RMH: recent modern humans. Due to strong fossilization, the Vrpc of 3 HEJ specimens cannot be segmented.

Figure 5. Between-group PCA of the deformation-based shape comparisons of premolar roots. Distal (left and upper ones at the X and Y axes, respectively) and lingual side (right and lower ones at the X and Y axes) of the extreme conformation of root shape are presented. Comparative groups are *H. erectus* from China (HEC), early *H. erectus* from Java (HEJ), Early Pleistocene *Homo* from North Africa (HNA), Neanderthals (NEA) and recent modern human (RMH).

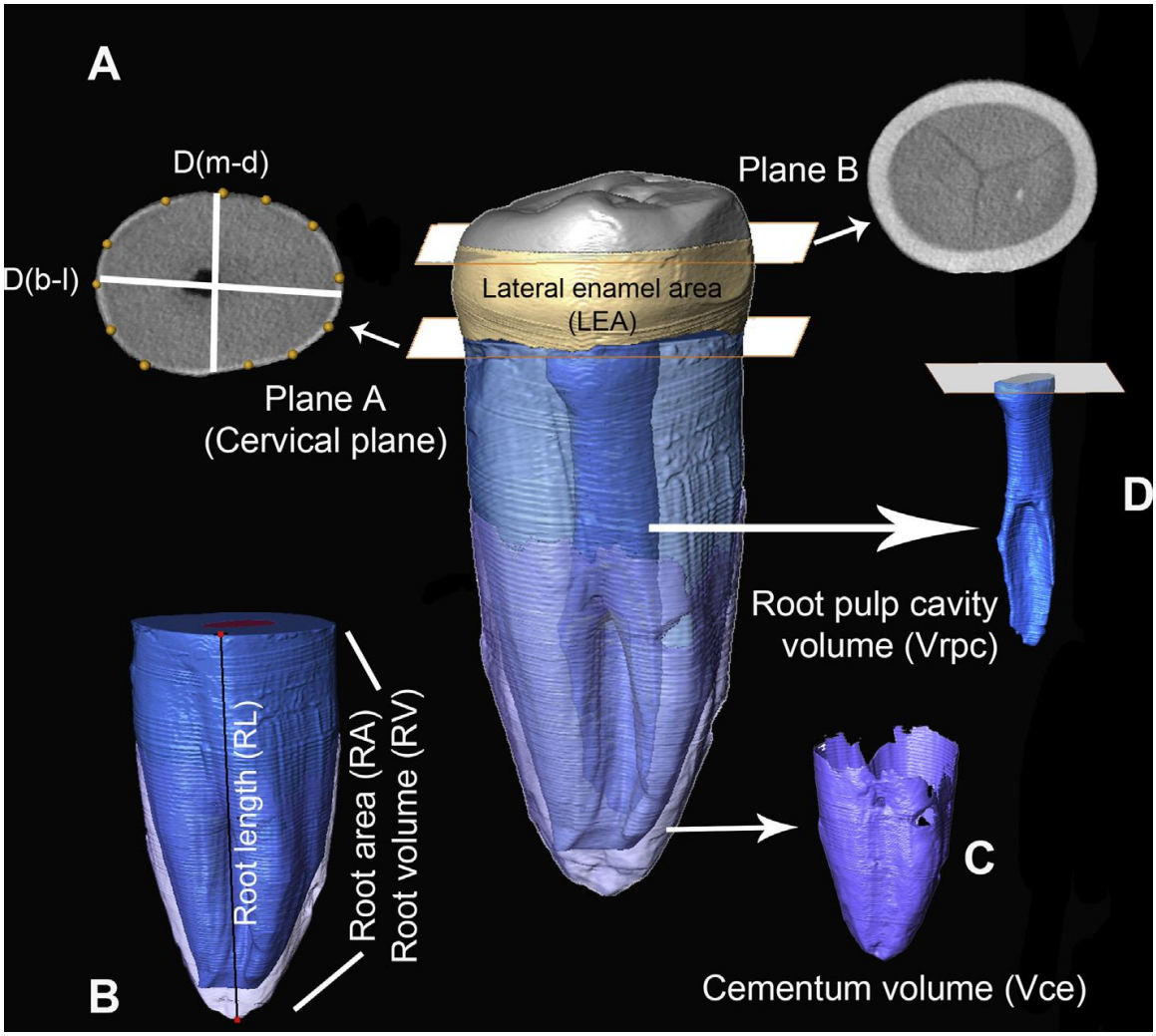
A
D(m-d)
D(b-l)
Plane A
(Cervical plane)
Plane B
Lateral enamel area
(LEA)
D
Root pulp cavity
volume (Vrpc)
C
Cementum volume (Vce)
B
Root length (RL)
Root area (RA)
Root volume (RV)

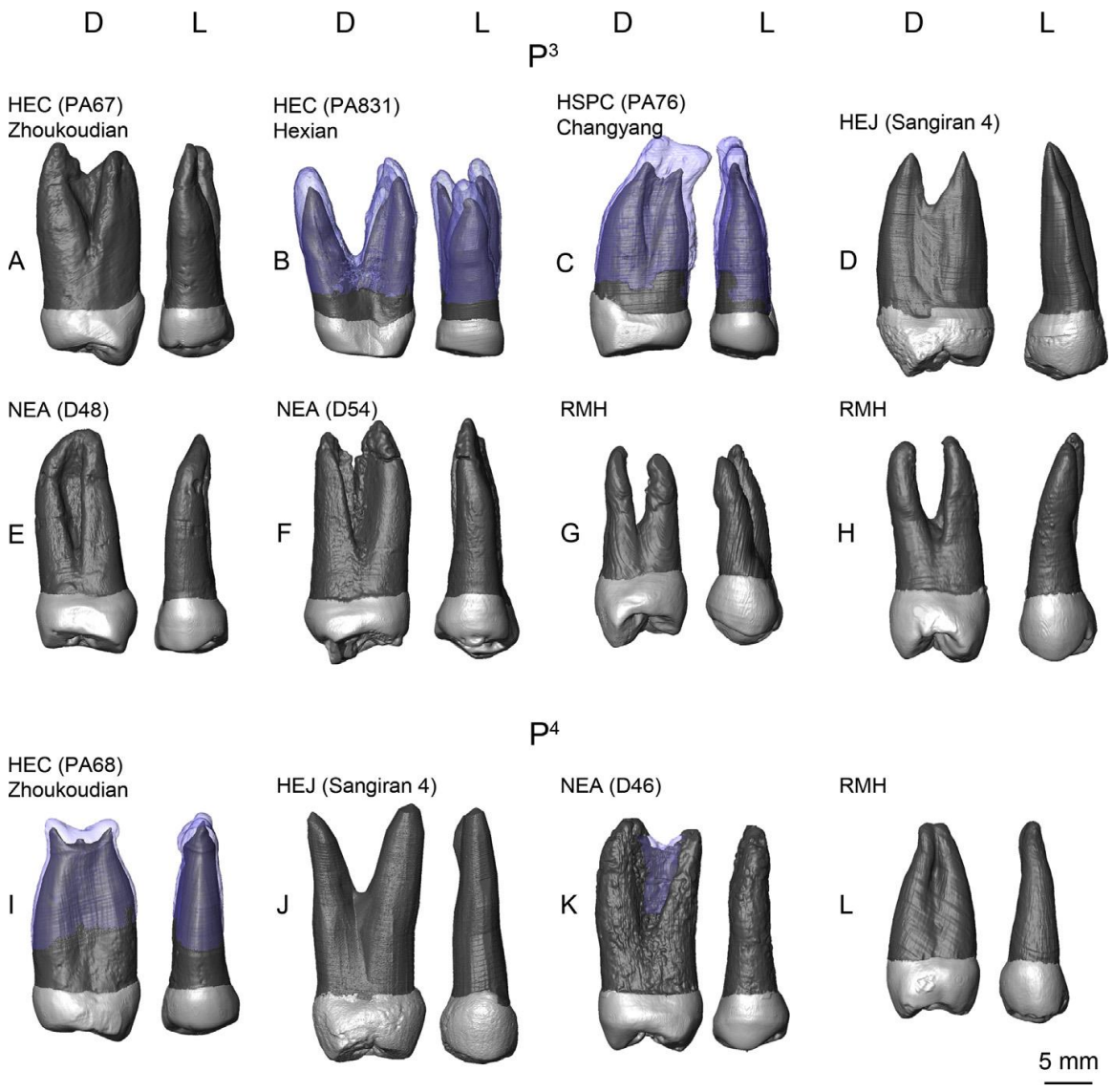
D
L
D
L
D
L
D
L
P3
HEC (PA67)
Zhoukoudian
HEC (PA831)
Hexian
HSPC (PA76)
Changyang
HEJ (Sangiran 4)
A
B
C
D
NEA (D48)
NEA (D54)
RMH
RMH
E
F
G
H
P4
HEC (PA68)
Zhoukoudian
HEJ (Sangiran 4)
NEA (D46)
RMH
I
J
K
L
5 mm

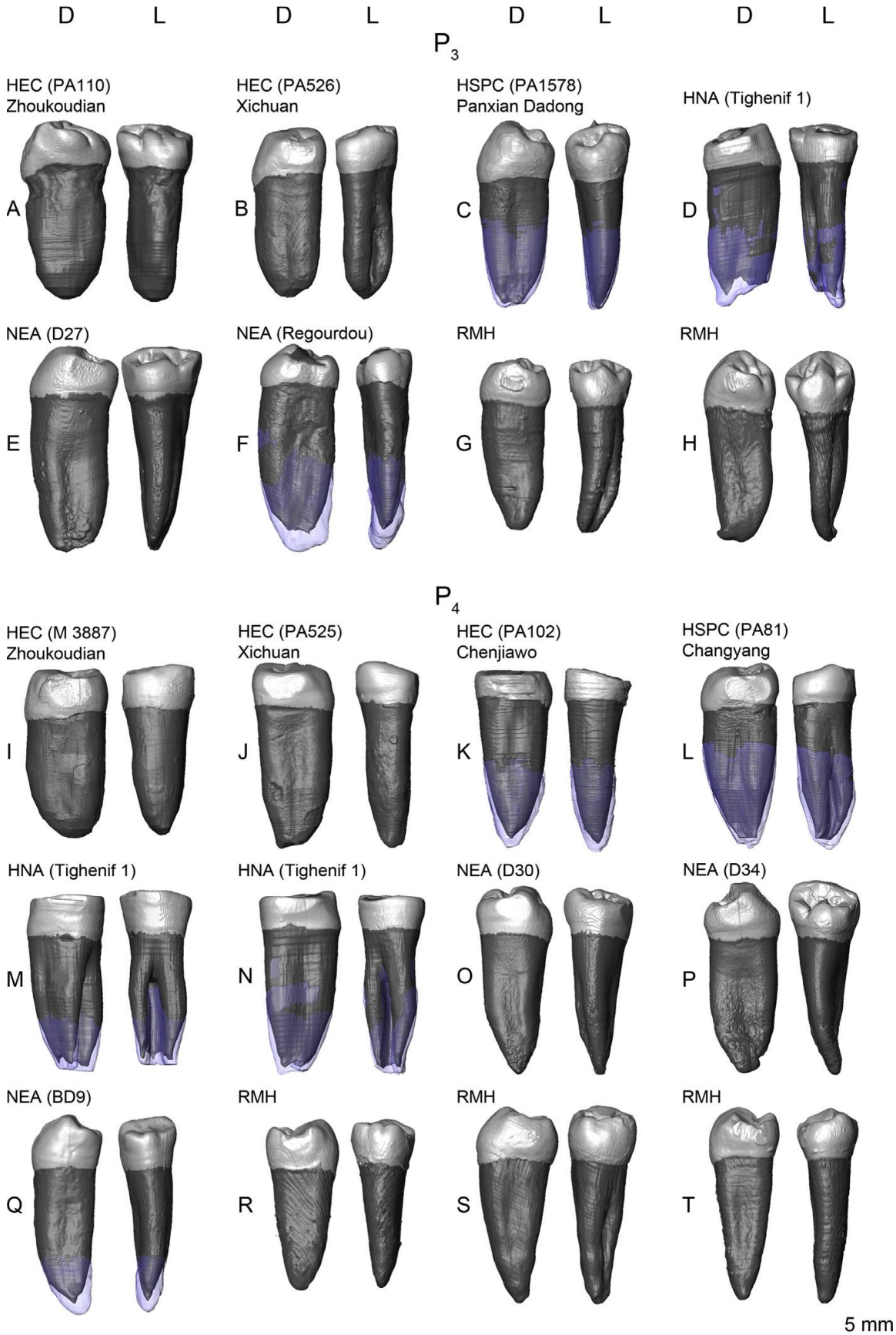
D L
D L
D L
D L
P3
HEC (PA110)
Zhoukoudian
A
HEC (PA526)
Xichuan
B
HSPC (PA1578)
Panxian Dadong
C
HNA (Tighenif 1)
D
NEA (D27)
E
NEA (Regourdou)
F
RMH
G
RMH
H
P4
HEC (M 3887)
Zhoukoudian
I
HEC (PA525)
Xichuan
J
HEC (PA102)
Chenjiawo
K
HSPC (PA81)
Changyang
L
HNA (Tighenif 1)
M
HNA (Tighenif 1)
N
NEA (D30)
O
NEA (D34)
P
NEA (BD9)
Q
RMH
R
RMH
S
RMH
T
5 mm

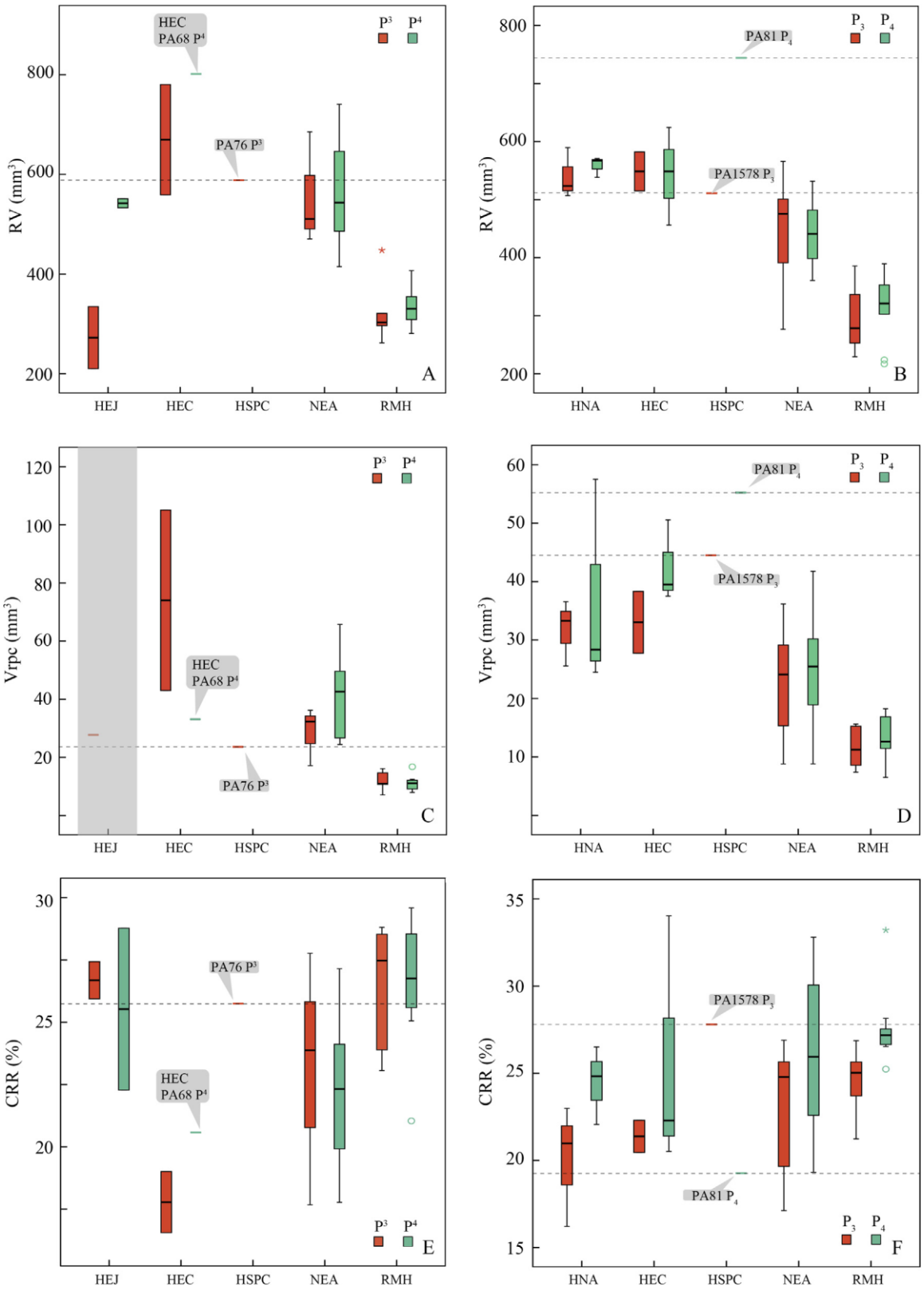
A
RV (mm³)
800
600
400
200
HEC
PA68 P⁴
PA76 P³
P³ P⁴
HEJ HEC HSPC NEA RMH
B
RV (mm³)
800
600
400
200
PA81 P4
PA1578 P3
P3 P4
HNA HEC HSPC NEA RMH
C
Vrpc (mm³)
120
100
80
60
40
20
HEC
PA68 P⁴
PA76 P³
P³ P⁴
HEJ HEC HSPC NEA RMH
D
Vrpc (mm³)
60
50
40
30
20
10
PA81 P4
PA1578 P3
P3 P4
HNA HEC HSPC NEA RMH
E
CRR (%)
30
25
20
PA76 P³
HEC
PA68 P⁴
P³ P⁴
HEJ HEC HSPC NEA RMH
F
CRR (%)
35
30
25
20
15
PA1578 P3
PA81 P4
P3 P4
HNA HEC HSPC NEA RMH

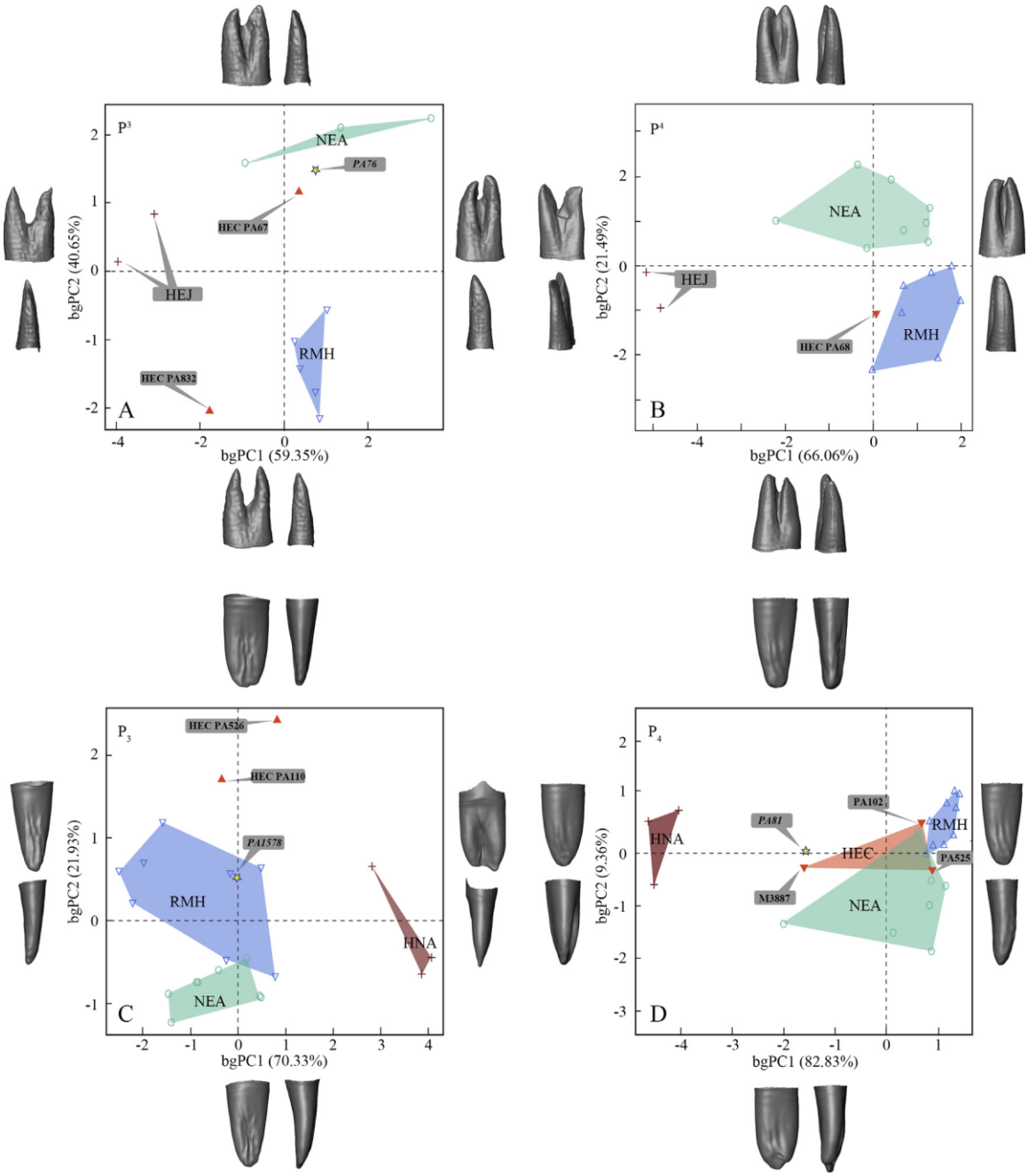
P³
NEA
PA76
HEC PA67
HEJ
RMH
HEC PA832
A
bgPC2 (40.65%)
bgPC1 (59.35%)
P⁴
NEA
HEJ
HEC PA68
RMH
B
bgPC2 (21.49%)
bgPC1 (66.06%)
P3
HEC PA526
HEC PA110
PA1578
RMH
HNA
NEA
C
bgPC2 (21.93%)
bgPC1 (70.33%)
P4
PA102
PA481
HNA
RMH
HEC
PA525
M3887
NEA
D
bgPC2 (9.36%)
bgPC1 (82.83%)